Invariant Characterization of Szekeres Models with Positive Cosmological Constant

N. T. Layden *[1], A. A. Coley †[2], and D. D. McNutt ‡[3]

[1,2]Department of Mathematics and Statistics, Dalhousie University, Halifax, Nova Scotia, Canada B3H 3J5
[3]Faculty of Science and Technology, University of Stavanger, N-4036 Stavanger, Norway

Abstract

We present an invariant characterization of black holes in the Szekeres spacetime with positive cosmological constant. In the formation of the black holes, we locate geometric horizons, and show that they coincide with the more traditional apparent horizons in the Szekeres models. We also define an invariant approach for detecting shell crossings. It is shown that shell crossing regions in the Szekeres models can be contained within the geometric horizons for situations where no naked singularities form, allowing for the study of astrophysical models that are inhomogeneous and with a cosmological constant. A measure of inhomogeneity through the dipole functions in the Szekeres models is used to compute shell crossing surfaces along particular directions in the spacetime. An example of the method applied to the axially symmetric collapse of a quasispherical dust is given, motivated by previous work on primordial black hole formation. Future extensions and generalizations of this work are also discussed.

Keywords— General Relativity, Black Hole Formation, Invariant Classification, Apparent Horizons

1 Introduction

The quasi-spherical Szekeres models are inhomogeneous solutions to Einstein's field equations that admit a perfect fluid source, with homogeneous pressure, and can include a cosmological constant [21, 20]. These models assume no symmetries in the spacetime, and hence are used as generalizations of the Lemaître-Tolman-Bondi (LTB) models that do not contain homogeneity, but are isotropic

*Nicholas.Layden@dal.ca
†Alan.Coley@dal.ca
‡david.d.mcnutt@uis.no

and spherically symmetric about a common center. The subfamilies of the Szekeres spacetime include Friedmann-Lemaître-Robertson-Walker (FLRW), Schwarzschild, de-Sitter, and LTB. The family of Szekeres models are characterized by an irrotational geodesic flow, a Petrov Type D Weyl tensor, and a shear tensor with two equal eigenvalues and eigensurface that coincides with the gravitoelectric part of the Weyl tensor [10, 18, 23]. Due to the lack of pressure gradients in the spatial coordinates, these models are also a special type of cosmological models called silent universes, where all worldlines are geodesic lines, and do not interact with neighbouring worldlines [9].

Following conjectures on geometric horizons [7], it has been shown for some exact solutions that special surfaces in a spacetime can be located through determining the zero set of certain curvature invariants in an invariant frame, which are referred to as geometric horizons. It has been shown that these geometric horizons coincide with the apparent horizons (properly referred to as marginally outer trapping surfaces) in other work [3]. With the inclusion of a positive cosmological constant, the equations in the Szekeres models need to be solved numerically except for certain subcases, and additional attention needs to be paid to tracking shell crossings in these collapsing models to develop physically reasonable models.

A full invariant characterization of the quasispherical Szekeres spacetime is given by [6]. Following the same procedure, given the Szekeres spacetime in the LT-type parameterization, we can utilize the Cartan invariants to describe the properties of the formation of the black holes. For this model to fit in with the theme of black hole collapse, we consider a situation where the model has a FLRW background, with a central overdense region that starts to collapse into a black hole, and another with a constant density. Motivated by previous work in primordial black hole formation [6, 13], we use similar examples of initial data to show how the method applies to collapsing models. An example of black hole formation is given, and is a qualitative example of applying the methods discussed here, and in principle the method applies to any example valid in the Szekeres models.

Previous work on analyzing the apparent horizons in the Szekeres spacetime [14, 18, 16, 4, 2, 19] have characterized the spacetimes as exact solutions without a cosmological constant. We formulate a more generalized model of the formation of black holes in the Szekeres spacetime embedded in a background spacetime with positive cosmological constant, and analyze the formation of multiple geometric horizons due to the presence of the cosmological constant. Since the cosmological constant in general does not allow for exactly integrable solutions in the Szekeres models except in very special cases, a numerical approach is required.

2 Szekeres Models

The standard line element for the Szekeres models can be written as

$$ds^2 = -dt^2 + e^{2\alpha}dz^2 + e^{2\beta}(dx^2 + dy^2), \tag{1}$$

where $\alpha(t, z, x, y)$, and $\beta(t, z, x, y)$ are determined by the Einstein Field Equations with an irrotational dust source. There are two classes of Szekeres models, Type I: $\beta_{,z} \neq 0$, and Type II: $\beta_{,z} = 0$. In general, these two classes need to be discussed separately. For this work, we will only discuss the $\beta_{,z} \neq 0$ class of spacetimes.

2.1 LT-type Szekeres Metric

In the LT type parameterization of the Szekeres metric, we have the line element in stereographic projective coordinates (t, r, p, q)

$$ds^2 = -dt^2 + \frac{\left(R' - \frac{RH'}{H}\right)^2}{\epsilon + 2E} dr^2 + \frac{R^2}{H^2}(dp^2 + dq^2) \tag{2}$$

where the metric functions $R(t, r)$, $H(r, p, q)$, are the areal radius and a dipole term to introduce inhomogeneities to the spacetime respectively, and we use the notation $' \equiv \frac{\partial}{\partial r}$ and $\dot{} \equiv \frac{\partial}{\partial t}$. The parameter ϵ determines the geometry of the solutions, $\epsilon = +1$ is quasi-spherical, $\epsilon = 0$ is quasi-planar, and $\epsilon = -1$ is pseudo-spherical. We will restrict our analysis to the quasi-spherical $\epsilon = +1$ case.

$$\begin{aligned} H(r, p, q) &= A(p^2 + q^2) + 2B_1 p + 2B_2 q + C, \\ AC - B_1^2 - B_2^2 &= \frac{1}{4}, \epsilon \end{aligned} \tag{3}$$

The functions $A(r), B_1(r), B_2(r), C(r)$ depend only on the radial coordinate r. And we cannot have $A(r) = 0$ or $C(r) = 0$ for $\epsilon = +1$ models, else the constraints are not satisfiable for real valued $B_1,\ B_2$. To keep the Lorentzian signature of the metric, we require that the function $E(r)$ satisfies:

$$E(r) \geq -\frac{1}{2} \tag{4}$$

Imposing the field equations on this model gives a Friedmann equation for $R(t, r)$ and a second equation for the density:

$$\dot{R}^2 = \frac{2M}{R} + 2E + \frac{\Lambda R^2}{3}, \tag{5}$$

$$4\pi\tilde{\rho} = \frac{\bar{M}'}{Y^2 Y'} = \frac{M' - 3MH'/H}{R^2(R' - RH/H)}. \tag{6}$$

The functions $\bar{M}, Y$ above are obtained from $\bar{M} \equiv \frac{M}{H^3}$, $Y \equiv \frac{R}{H}$. The function $M(r)$ is an arbitrary function of integration of the field equations. This function $M(r)$ will be one of the functions necessary to fully specify a model. Integrating equation (5) gives us another arbitrary function:

$$t - t_B(r) = \pm \int_0^R \frac{d\tilde{R}}{\sqrt{\frac{2M}{\tilde{R}} + 2E + \frac{\Lambda \tilde{R}^2}{3}}}, \tag{7}$$

A full solution to the Friedmann equation (5) in terms of elliptic functions of the third kind is given in [1]. In analogy to the LTB solution, we have three LT-type functions to specify for a model:

$$E(r), \quad t_B(r), \quad M(r), \tag{8}$$

where we can interpret the functions analogously to the LTB models. $E(r)$ is the energy per unit mass in each shell, the sign of $E(r)$ determines the type of evolution in the spacetime. The function $t_B(r)$ is the bang or crunch time function, which defines the spatial dependence of the big bang and

can be determined by setting $t = 0$ and integrating (7). $M(r)$ is the gravitational mass of each shell at coordinate radius r, in the quasi-spherical spacetime this is the total gravitational mass inside the sphere of radius r, though it is not the same as the mass contained in the sphere.
From the constraints in equations (3), we can rearrange the dipole term to write it as [15]

$$H(r,p,q) = \frac{S}{2}\left[\left(\frac{p-P}{S}\right)^2 + \left(\frac{q-Q}{S}\right)^2 + 1\right], \tag{9}$$

the functions $S(r), P(r), Q(r)$ are arbitrary functions, and are related to the constraints in (3) by:

$$\begin{gathered} A = \frac{1}{2S}, \quad B_1 = \frac{-P}{2S}, \quad B_2 = \frac{-Q}{2S}, \\ C = \frac{P^2+Q^2+S^2}{2S}. \end{gathered} \tag{10}$$

We have introduced 3 more arbitrary functions, bringing the set of functions necessary to define a model to 5 with a 6th function used to rescale the r coordinate.

$$\begin{gathered} E(r), \quad t_B(r), \quad M(r), \\ S(r), \quad P(r), \quad Q(r), \end{gathered} \tag{11}$$

The functions S, P, Q effectively set the dipole distribution of the matter in the comoving coordinates.

2.2 Solution to the Marginally Bound Model

The marginally bound model is exactly solvable for the Szekeres/LTB Friedmann equation (5), corresponding to the case with $E(r) = 0$. Previously, this solution was given in these coordinates in [1]. The solution is a simple hyperbolic trigonometric function:

$$\dot{R}^2 = \frac{2M}{R} + \frac{\Lambda}{3}R^2, \tag{12}$$

$$R(t,r) = \left(\frac{6M}{\Lambda}\right)^{1/3} \sinh^{2/3}\left(\iota\sqrt{\frac{3\Lambda}{4}}(t - t_B(r))\right), \tag{13}$$

$$t_B(r) = -\iota\sqrt{\frac{4}{3\Lambda}}\,\sinh^{-1}\left(\sqrt{\frac{\Lambda R_0^3}{6M}}\right), \tag{14}$$

where $R(0,r) = R_0$ is the initial scaling (typically set to $R(0,r) = r$ due to the scaling freedom of r in the metric coordinates), and $\iota = +1, -1$ corresponds to the exploding and imploding solutions of (12) respectively.

We also include the various derivatives of $R(t,r)$ for completeness:

$$\dot{R} = \iota\sqrt{\frac{\Lambda}{3}}R\,\coth\left(\iota\sqrt{\frac{3M}{4}}(t - t_B)\right), \tag{15}$$

$$R' = R\left[\frac{M'}{3M} + \iota\sqrt{\frac{\Lambda}{3}}\,t'_B\,\coth\left(\iota\sqrt{\frac{3M}{4}}(t - t_B)\right)\right]. \tag{16}$$

There has been a history of work done on these marginally bound exact solutions for various phenomena, and they can be useful to aid the numerical analysis when introducing $E(r) \neq 0$. This set of solutions is also useful when constructing models where $E(r)$ changes sign in the domain, as all regions separated by $E(r) = 0$ can be matched numerically to these exact solutions.

2.3 Invariant Classification of the Szekeres Spacetime

We summarize the results in [6] for classifying the Szekeres spacetime in terms of Cartan invariants by using the Cartan-Karlhede algorithm here. The invariant coframe determined by the Cartan-Karlhede algorithm for the Szekeres metric in terms of a complex null tetrad of covectors is:

$$g = -2\ell_{(a}n_{b)} + 2m_{(a}\bar{m}_{b)} \tag{17}$$

where the round brackets denote the symmetrization of the indices, and

$$\ell_a = \frac{1}{\sqrt{2}}\left(dt + \frac{HY'}{\sqrt{1+2E}}dr\right),\ n_a = \frac{1}{\sqrt{2}}\left(dt - \frac{HY'}{\sqrt{1+2E}}dr\right), \tag{18}$$

$$m_a = \frac{Y}{\sqrt{2}}(dx - idy),\ \bar{m}_a = \frac{Y}{\sqrt{2}}(dx + idy), \tag{19}$$

and the dual frame vectors are $\{n^a, \ell^a, \bar{m}^a, m^a\}$, such that $-\ell^a n_a = m^a \bar{m}_a = 1$, and all vectors are null, $\ell^a \ell_a = n^a n_a = m^a m_a = \bar{m}^a \bar{m}_a = 0$. The Ricci-Newman-Penrose scalars are related by

$${}^4\mathcal{R} = 4\Phi_{00},\ \Phi_{22} = \Phi_{00},\ \Phi_{11} = \frac{1}{2}\Phi_{00}. \tag{20}$$

The non-trivial Newman-Penrose (NP) curvature scalars in terms of the metric functions are

$$\Phi_{00} = \frac{\tilde{\rho}}{\kappa} = \frac{2(M' - 3MH'/H)}{R^2(R' - RH'/H)},\ \Psi_2 = -\frac{M' - 3MH'/H}{2(R/H)^3} + \frac{\kappa}{12}\tilde{\rho},\ \text{where } \kappa = \frac{8\pi \mathrm{G}}{\mathrm{c}^4} = 8\pi. \tag{21}$$

The Weyl tensor is of type II/D, and the Ricci tensor is of Type I relative to the alignment classification [5]. The non-zero spin-coefficients are:

$$\rho = \frac{1}{\sqrt{2}}\left(\frac{\dot{R} - \sqrt{1+2E}}{R}\right),\ \mu = -\frac{1}{\sqrt{2}}\left(\frac{\dot{R} + \sqrt{1+2E}}{R}\right), \tag{22}$$

$$\gamma = -\epsilon = \frac{1}{2\sqrt{2}}\frac{\dot{Y}'}{Y'},\ \tau = \bar{\nu} = -\tilde{\kappa} = -\bar{\tilde{\pi}} = -\frac{i}{2\sqrt{2}}\left(\frac{(HY')_{,q} - i(HY')_{,p}}{HYY'}\right). \tag{23}$$

The covariant derivative of the Weyl tensor yields the following terms with positive boost weight:

$$C_{1214;3} = C_{1434;3} = C_{1213;4} = C_{1334;4} = 3\rho\Psi_2, \tag{24}$$

$$2C_{1423;1} = C_{1212;1} = C_{3434;1} = \frac{-2\Delta\Phi_{11} - 32\epsilon\Phi_{11} - 4\mu\Phi_{11} + \rho(18\Psi_2 + 4\Phi_{11})}{3}. \tag{25}$$

with Δ being the covariant derivative operator in the direction of the tetrad vector n^a, $\Delta \equiv \nabla_n$.

2.4 Kinematic Quantities of the 1+3 Fluid Flow Approach

For the kinematic quantities of the comoving dust fluid, we have the following variables, in terms of the Cartan invariants, and the metric functions [6, 19, 9]:

$$\tilde{\rho} = \frac{\kappa}{2}\Phi_{22} = \frac{2\,(M' - 3MH'/H)}{\kappa R^2\,(R' - RH'/H)}, \tag{26}$$

$${}^3\mathcal{R} = 18\Phi_{22}, \tag{27}$$

$$\mathcal{W} = 2\Psi_2 = \frac{M}{3R^3}\frac{3R' - RM'/M}{R' - RH'/H}, \tag{28}$$

$$\Theta = -\frac{\sqrt{2}}{2}(2\epsilon - \rho + \mu) = \frac{\dot{R}' + 2\dot{R}R'/R - 3\dot{R}H'/H}{R' - RH'/H}, \tag{29}$$

$$\Sigma = \frac{\sqrt{2}}{6}(4\epsilon + \rho - \mu) = -\frac{1}{3}\frac{\dot{R}' - \dot{R}R'/R}{R' - RH'/H}, \tag{30}$$

where $\tilde{\rho}$ is the fluid energy density, ${}^3\mathcal{R}$ is the Ricci scalar curvature of t=const hypersurfaces orthogonal to the fluid velocity, u^a, $\mathcal{W}$ is the electric Weyl scalar, Θ is the expansion scalar, and Σ is the shear scalar. The terms (26) - (30) can be assembled into the 1+3 covariant evolution equations, including a cosmological constant:

$$\tilde{\rho}_{,t} = -\Theta\tilde{\rho}, \tag{31}$$

$$\Theta_{,t} = -\frac{\Theta^2}{3} - \frac{\kappa}{2}\tilde{\rho} - 6\Sigma^2 + \Lambda, \tag{32}$$

$$\Sigma_{,t} = -\frac{2}{3}\Theta\Sigma - \Sigma^2 + \mathcal{W}, \tag{33}$$

$$\mathcal{W}_{,t} = -\Theta\mathcal{W} - \frac{\kappa}{2}\tilde{\rho}\Sigma + 3\Sigma\mathcal{W}, \tag{34}$$

subject to the Hamiltonian and spacelike constraints, including a cosmological constant modified from Sussman and Bolejko's equations [19]:

$$\frac{\Theta^2}{9} = \frac{\kappa\tilde{\rho}}{3} - \frac{{}^3\mathcal{R}}{6} + \Sigma^2 + \frac{\Lambda}{3}, \tag{35}$$

$$\bar{\nabla}_b\sigma^b_a - \frac{2}{3}h^b_a\Theta_{,b} = 0, \tag{36}$$

$$\bar{\nabla}_b W^b_a - \frac{\kappa}{3}h^b_a\rho_{,b} = 0. \tag{37}$$

2.5 Subspaces of the Szekeres dynamical models

Given the set of covariant evolution equations (31)-(34) for the dynamics of Szekeres models, in addition to the Hamiltonian and spacelike constraints, we can identify conditions on the equations

that produce a FLRW model. A vanishing Weyl tensor identifies the family of FLRW models. In the Szekeres models, this corresponds to the vanishing of the electric Weyl scalar (28). Now given equation (34) for the evolution of the electric Weyl scalar, if we have an initial hypersurface with $\mathcal{W} = 0$, to keep a flat geometry, we necessarily require zero shear as well. This is a well known condition that vanishing shear results in a family of FLRW models. Due to the coupling of the evolution of the shear scalar and Weyl scalar through equation (33), we then note that the initial data must not contain both vanishing shear and vanishing electric Weyl scalar simultaneously, else we are immediately restricted to FLRW evolution along each worldline. For the shear scalar in terms of the metric functions in (30), an initial zero shear surface corresponds to the numerator vanishing:

$$\Sigma = 0 \implies \dot{R}' = \dot{R}R'/R. \tag{38}$$

Using the Friedmann equation (5), we find an expression for the vanishing of the shear to be a solution to:

$$3MR' + 2ERR' - R^2E' - RM' = 0. \tag{39}$$

which has a solution for R in terms of M and E:

$$R(t,r)|_{\Sigma=0} = \begin{cases} -\frac{M}{E} & \text{if } E < 0 \\ \frac{M}{E} & \text{if } E > 0 \end{cases} \tag{40}$$

The expressions above also appear in LTB and Szekeres models as the characteristic length scale for $\Lambda = 0$, as in [14]. In the case of $\Lambda = 0$, this condition corresponds to a critical value of the Friedmann equation (5), and is unphysical in those models. When $\Lambda = 0$, this expression is the maximum expansion of R for each worldline. For the case of non-zero cosmological constant, we can have a surface of zero shear existing in the model at some time which is not a critical value for the Friedmann equation for R. Observing the covariant evolution equations for the Szekeres models, we see that initial conditions can exist initially with zero shear, as long as the Weyl curvature scalar is non-zero as well, as the coupling of equations (33) and (34) will introduce shear or Weyl curvature as long as neither are simultaneously zero. Similarly, initial conditions can contain zero Weyl curvature initially, with non-zero shear, so that we avoid the FLRW models. Thus we must be careful in defining initial conditions to avoid any situation where the shear and electric weyl scalars are zero on some worldline in the domain. This condition requires modifying either the forms of the metric functions M and E so any initial data does not coincide, or rescaling the initial conditions using the bang time function, t_B. If the zero shear condition holds for all t, this implies that the areal radius $R(t,r)$ is separable and thus defines a FLRW family as a subset of the Szekeres models.

The existence of special surfaces in the Szekeres spacetime with vanishing shear and Weyl curvature allows the existence of special homogeneous slices of the spacetime that preserve their inhomogeneity for all time. This feature of the Szekeres models has been discussed in [10] and allows for regions for matching multiple Szekeres regions to other regions in the spacetime.

3 Shell Crossings

Shell crossing singularities in the Szekeres models occur (in the LTB parameterization) when the g_{rr} metric function vanishes.

$$\sqrt{g_{rr}} = \frac{\left(R' - R\frac{H'}{H}\right)}{\sqrt{1+2E}} = 0, \tag{41}$$

For regularity conditions, we require the denominator term to be positive definite via conditions on E. The vanishing of (41) also corresponds to the energy density function becoming singular, from equation (6). Thus we can get a simple expression for the first occurrence of a shell crossing as

$$\frac{R'}{R} = \frac{H'}{H}. \tag{42}$$

And from the work done by Hellaby et al. [15], they showed that a tighter constraint on the existence of the shell crossings is given by making sure that $\frac{R'}{R}$ is greater than the maximum of the dipole term. For no shell crossings to exist, it requires:

$$\frac{R'}{R} > \left.\frac{H'}{H}\right|_{max}. \tag{43}$$

Where $H'/H|_{max}$ is given by the expression:

$$\left.\frac{H'}{H}\right|_{max} = \frac{\sqrt{S'^2 + P'^2 + Q'^2}}{S} \tag{44}$$

It would then be necessary to track the time evolution of the term $\frac{R'}{R}$ to determine if a shell crossing has occurred after some time in a given model.

We define the term

$$\zeta \equiv \frac{R'}{R}, \tag{45}$$

Then take the time derivative of ζ to study the time evolution.

$$\dot{\zeta} = \frac{\dot{R}'R - \dot{R}R'}{R^2}. \tag{46}$$

For some physical considerations on the expected dynamics of ζ, in a collapsing model, we know the signs of the terms. With collapse, $\dot{R} < 0$ is always true. $R' > 0$ must be true for the density to be non-negative and finite. $R \geq 0$ because the areal radius being negative has no physical significance. And since the shells are drifting from a quantity larger than the dipole maximum, towards a shell crossing, then the time rate of change of ζ should be negative, or potentially zero, which we will study the consequences of. If we imagine ourselves in the collapsing LTB case, then the quantity R' decreases towards zero before the shells cross at $R' = 0$, indicating that the term $\dot{R}' \leq 0$. For $\dot{\zeta} < 0$, we then require that $\dot{R}'R < -\dot{R}R'$

3.1 Stationary solutions to $\dot{\zeta}$

In the special case where $\dot{\zeta} = 0$, the term $\frac{R'}{R}$ is constant for all time, and this corresponds exactly to the FLRW subcase of these models, which is expected because the vanishing of this parameter also corresponds directly to the vanishing of the shear. The condition for these models to reduce to

FLRW is that the areal radius, the 'scale factor', be separable. Let us suppose $R(t,r) = F(r)a(t)$, then

$$\dot{\zeta} = \frac{F'\dot{a}Fa - F'aF\dot{a}}{F^2a^2} \equiv 0. \tag{47}$$

Thus, when $\dot{\zeta} = 0$, the evolution of R'/R is equivalent to the FLRW subcase, since $\dot{\zeta}$ vanishes identically. Moreover, we can find the conditions on which our initial data is on an FLRW subspace. Expanding equation (46) using the evolution equation (5), we arrive at a differential equation, which has a solution for when $\dot{\zeta} = 0$, which corresponds to $R(t,r)$ being related to $M(r)$ and $E(r)$ as:

$$R(t,r) = \frac{-M(r)}{E(r)}a(t), \tag{48}$$

where $a(t)$ is the FLRW scale factor. In [14], the quantity $-M/E$ ($M/|E|$ solves the 'zero shear' term for $E \neq 0$) can be regarded as a characteristic length scale in the LTB models, which is consistent with the Szekeres models in the LT parameterization.

3.2 Shell Crossing 'Evolution' Equation

To locate shell crossings when numerically integrating the field equations, we also need to compute the r-derivative of $R(t,r)$, so we introduce another ODE derived from the Friedmann equation (5):

$$\dot{R}' = \frac{1}{\dot{R}}\left(\frac{M'R - MR'}{R^2} + E' + \frac{\Lambda}{3}RR'\right). \tag{49}$$

This equation can be integrated alongside the Friedmann equation to calculate the time evolution of R'. In the case where initial conditions are $R(0,r) = r$, this reduces to $R'(0,r) = 1$.

4 Defining Model Parameters

To fully specify a Szekeres model, we require the LTB functions $t_B(r),\ M(r),\ E(r)$ and the dipole functions $S(r),\ P(r),\ Q(r)$. Here we provide generic functional forms for the model functions to examine the occurrence of shell crossings in black hole models.

4.1 LTB Functions

For the collapse/bang function, we choose an initial scaling $R(0,r) = R_0$ and compute it with the integral

$$t_c(r) = \int_0^{R_0} \frac{dR}{\sqrt{\frac{2M}{R} + 2E + \frac{\Lambda R^2}{3}}}. \tag{50}$$

This integral needs to be integrated numerically for each model, and is done so by using a generic quadrature method. Alternatively, the collapse time function can be determined numerically in a collapsing model by solving the evolution equation (5) and determining the time each worldline takes to reach $R = 0$, which in general will give an approximate collapse time since the integrators will fail when R is near zero. However, with sufficiently high precision time steps the collapse time

function will be similar to the integral as expected. For any given collapse function, it is clear that if $t_c(r)$ contains maxima or minima anywhere on the domain of the r coordinate, we expect shell crossings to occur, at least at late times. Additionally, if $t_c'(r) < 0$ inside the domain, this implies that the outer shells collapse through (in the LTB sense) all inner shells until the crunch time.
The energy functions are all for the elliptic type of evolution, with $E(r) < 0$, and for regularity of the energy function, we have the conditions $E(0) = 0$, $E \geq -1/2$, motivated by previous work by Harada and Jhingan [12], we will include their 'Model D', and modifications for $E(r)$:

$$E_1(r) = \begin{cases} \left(\frac{r}{r_c}\right)^2 \left(1 + \left(\frac{r}{r_w}\right)^{n_1} - 2\left(\frac{r}{r_w}\right)^{n_2}\right)^4 & \text{if } 0 \leq r \leq r_w \\ 0 & \text{if } r \geq r_w. \end{cases} \tag{51}$$

where r_b is another parameter used to move the energy curve around the domain of r. And we also take $r_w = 1$, $r_c = 10$, and vary $n_1,\ n_2$.

4.2 Mass and Density Profiles

For the mass and density in a model, given an initial scaling, we can opt to specify a density profile and compute the mass from it by integrating the density equation (6) along the direction where the dipole term vanishes $H'/H = 0$, since $M(r)$ is a function of a single variable. Given a density profile, and an initial scaling $R(0, r) = r$, the mass is computed by the integral of

$$M'(r) = \frac{\kappa}{2}\rho_L r^2, \tag{52}$$

$$M(r) = \frac{\kappa}{2}\int_0^r \rho_L \tilde{r}^2 d\tilde{r}. \tag{53}$$

where ρ_L is the equivalent to an LTB density profile along the direction $H'/H = 0$, motivated by the work of Vrba and Svitek [22], when it comes to cosmological applications, it might be more insightful to specify density profiles and a density contrast when constructing models, and generalized exact perturbations from FLRW models.

We define density profiles in the spacetime, to study the appearance of shell crossings and the horizons:

$$\rho_L = \frac{3}{\kappa}, \tag{54}$$

$$\rho_L = ae^{-(br)^2} + c, \tag{55}$$

$$\rho_L = a\tanh(b(r-c)) + d. \tag{56}$$

The constants a, b, c, d in the above equations are chosen to see the behaviour of the collapse in each of the density profiles, and monitor the appearance of shell crossings.

4.3 Dipole Functions

For the dipole terms, we choose a set of generic functions for the dipole:

$$S(r) = e^{-\alpha r},\ P(r) = Q(r) = B, \tag{57}$$

where the exponent $\alpha \in [0, 1)$, and B a positive real constant. Since B is a constant in this case, these dipole functions define an axially symmetric subcase. Varying the parameter α tells us how strong we can make a dipole and still keep the shell crossings behind the horizon. We keep $\alpha < 1$ so that there are no shell crossings on the initial data set. The case of $\alpha = 0$ is equivalent to $S(r) = 1$, which corresponds to the LTB subcase of these models (up to appropriate rescaling).

5 Invariantly Defined Horizon Structure

We have shown in [6] that the extended Cartan invariant ρ determines the location of the geometric horizons due to its presence in the covariant derivative of the Weyl tensor (24), defining an algebraically special surface. In previous work on the structure of the apparent horizons in the quasi-spherical Szekeres models [4], we showed that the geometric horizon coincides with the apparent horizon. This shows us that the apparent horizon in these Szekeres models is an invariantly defined, algebraically special surface in the spacetime.

The extended Cartan invariant ρ is given by

$$\rho = \frac{\dot{R} - \sqrt{1 + 2E}}{\sqrt{2}R}, \tag{58}$$

where the geometric horizon is defined by the surface $\rho = 0$, giving us the condition

$$\dot{R} = \sqrt{1 + 2E}. \tag{59}$$

We take the Friedmann equation for R, bringing in this condition for the horizon, giving an algebraic expression for the geometric horizon

$$\frac{2M}{R} + \frac{\Lambda R^2}{3} - 1 = 0. \tag{60}$$

Written in another way:

$$g(R) := \Lambda R^3 - 3R + 6M = 0. \tag{61}$$

In previous work on Szekeres models [17, 1, 11], the apparent and cosmological horizons were determined by an algebraic constraint equivalent to (61). This shows that the apparent horizons and cosmological horizons are geometric horizons in the Szekeres spacetime. For tracking the appearance of the geometric horizons in the spacetime, the Cartan invariant ρ locates the horizon in the expanding spacetime ($\dot{R} > 0$), and in the collapsing spacetime ($\dot{R} < 0$), the horizon is detected by the spin coefficient $\mu = 0$. Additionally, since $\rho = 0$ detects the horizon, (59) tells us that the expansion of R on the horizons is independent of time.

5.1 Locating the Horizons

From the algebraic expression for the horizon in (61), we can analyze the roots of this equation to determine the circumstances in which the horizon appears. The only two parameters that determine the number of roots of the cubic equation are $M(r)$ and Λ. We must have positive gravitational mass, $M(r) \geq 0$, and positive cosmological constant, $\Lambda > 0$. If we consider the locations of the critical points of (61) in terms of R:

$$3\Lambda R^2 - 3 = 0. \tag{62}$$

The critical points of the function are fixed depending on Λ:

$$R_{cp} = \pm\frac{1}{\sqrt{\Lambda}}. \tag{63}$$

The values of the critical points tells us that one of the three roots has to be negative, and it will be shown that for a single positive root to exist, this requires negative mass, violating our condition on $M(r)$ being positive. One of the roots will be negative, and is unphysical. The simplest case to deal with is when $\Lambda = 0$, which reduces the expression to $R_{gh} = 2M$, equivalent to the Schwarzschild radius. Taking $\Lambda > 0$, and $M(r) = 0$ gives two solutions, $R_{gh}|_{M=0} = \{0, \frac{\sqrt{3}}{\sqrt{\Lambda}}\}$, the second of which is similar to the de Sitter cosmological horizon. When the function $M(r)$ 'increases', it moves the image of $g(R)$ upward, bringing the two real roots together, and they meet at the critical point $R_{cp} = \frac{1}{\sqrt{\Lambda}}$. If $M(r)$ increases further, there will be no positive real roots of $g(R)$, therefore no horizon. The maximum restriction on $M(r)$ can be determined by equating the root and the critical point of $g(R)$.

$$\Lambda\frac{1}{\sqrt{\Lambda}^3} - 3\frac{1}{\sqrt{\Lambda}} + 6M = 0, \tag{64}$$

We then find that the restriction on $M(r)$ provides a critical value of $M(r)$ that determines the number of roots of $g(R)$, and thus the number of horizons in the spacetime.

$$M_{crit} := M(r)|_{r=R_{cp}} = \frac{1}{3\sqrt{\Lambda}}. \tag{65}$$

If $M(r) = M_{crit}$, there is only one horizon located at $R = \frac{1}{\sqrt{\Lambda}}$. If $M > M_{crit}$, there are no horizons (no positive real roots). And if $M < M_{crit}$, then there are two solutions, corresponding to the positive roots of the function $g(R)$, which can be written as

$$R_k = \frac{2}{\sqrt{\Lambda}} cos\left(\frac{\theta - 2\pi k}{3}\right), \tag{66}$$

where $cos(\theta) = -3M\sqrt{\Lambda}$, and $k = 0, 1$. The two roots correspond to a generalized cosmological horizon with $k = 0$, and $k = 1$ corresponds to the apparent horizon, both of which are invariantly defined by the Cartan invariant ρ. And a similar result is given in [4] for the apparent horizons they detect. A list of the different horizons that can form are given in Table 1. Thus each worldline in the spacetime can encounter either 0, 1 or 2 horizons throughout its evolution.

5.2 Timing the Horizons and Shell Crossings

To determine when and where the horizons appear in the spacetime, we can solve the Friedmann equation (5) and use the expressions for the areal radii of the horizons from Table (1) as follows:

$$t_{gh}(r) = -\int_0^{R_{gh}} \frac{dR}{\sqrt{\frac{2M}{R} + 2E + \frac{\Lambda R^2}{3}}} + t_c(r). \tag{67}$$

Table 1: All possible positive real roots of the function $g(R)$ (61) that detects the horizon. The critical value of M is given by $M_{crit} = \frac{1}{3\sqrt{\Lambda}}$, and θ is defined by $cos(\theta) = -3M\sqrt{\Lambda}$. The work done in [8] is comparable to our results, and a similar expression and discussion of roots of this cubic function are also found in [11]. When there are two positive real roots, $k = 0$ corresponds to the cosmological horizon, and $k = 1$ corresponds to the geometric/apparent horizon.

Condition	Geometric Horizons Admitted
$\Lambda = 0$	$R = 2M$
$M(r) = 0$	$R = \frac{\sqrt{3}}{\sqrt{\Lambda}}$, $R = 0$
$M(r) < M_{crit}$	$R_k = \frac{2}{\sqrt{\Lambda}} cos\left(\frac{\theta - 2\pi k}{3}\right)$, $k = 0, 1$
$M(r) = M_{crit}$	$R = \frac{1}{\sqrt{\Lambda}}$
$M(r) > M_{crit}$	No positive solution

The shell crossings on the other hand, must be determined by solving the Friedmann equation as an ODE from initial conditions, then compute $R'(t, r)$ to locate them. We locate the shell crossings by computing the zero set of the shell crossing detector

6 Models of Black Hole Formation

We present a model for black hole formation with a non-zero cosmological constant. Previous work on apparent horizons and shell crossings in this context for the Szekeres metrics were studied in [4, 11, 12, 17]. For a non-zero cosmological constant, shell crossing formation in Szekeres models can be censored by a geometric horizon in a collapsing region embedded in some exterior spacetime. The parameters that we focussed on are the 'energy' function $E(r)$, the cosmological constant Λ, and the non-sphericity functions that define the Szekeres dipole S, P and Q. These examples were motivated from the work done in [12], and can be interpreted as models of primordial black hole formation, but here they are used more in a qualitative sense for a general model of black hole formation. These models with cosmological constant make more sense in the context of late-time black hole formation. The numerical examples are presented in geometric units $c = G = 1$, and the emphasis of this choice is on the application of the geometric horizon detection.

6.1 Examples of Shell Crossing Profiles

We construct a set of models to examine shell crossing profiles numerically, with the dipole functions (57) and the density profiles (54), and display their horizon structure.

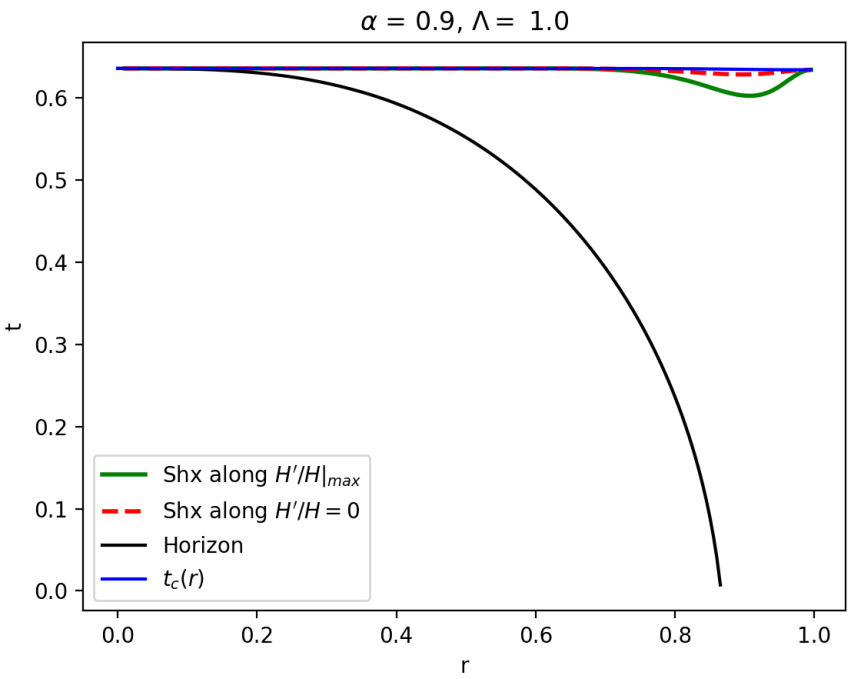

Figure 1: Model with $E(r)$ given by equation (51), $n_1 = 8, n_2 = 10$, where the dipole variation has $\alpha = 0.9$, $B = 0$, with positive cosmological constant $\Lambda = 0.01$, and the initial density given by the constant function in (54). This model is axially symmetric since $P = Q = 0$. The vertical axis is cosmic time, the worldlines of radial coordinate r are represented on the horizontal axis. The black line is the zero set of the horizon detector $\rho = 0$, the upper branch of the line is the geometric horizon, and the lower branch is the cosmological horizon, and both horizons connect on the right side of the domain at approximately $t = 0.86$. The blue line is the time until each worldline collapses to $R(t_c, r) = 0$, and the red and green lines are the LTB shell crossing and maximal dipole shell crossings, respectively. There are wordlines along which no horizon appears, but a shell crossing does appear, thus shell crossings are not fully censored by the geometric or cosmological horizon formations. The two directions for the shell crossings are shown since the shell crossings along the maximum of the dipole term will be the first to cross in these cases, and for $H'/H = 0$, we can see the LTB subcase for comparison. The coordinates (p, q) are thus suppressed in this graph. The focus is on the detection of the horizons and the shell crossing surfaces along particular directions.

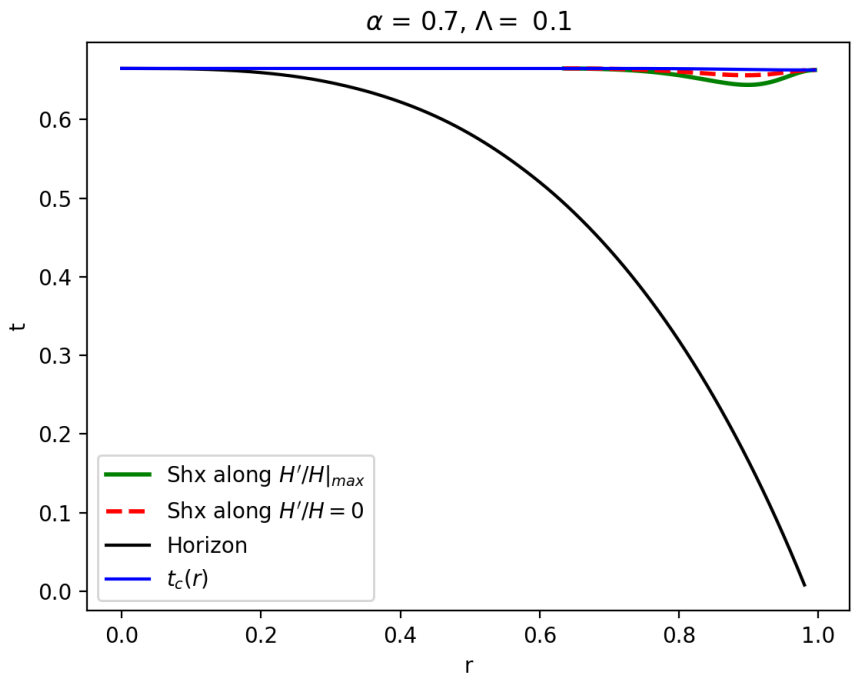

Figure 2: Model with $E(r)$ given by equation (51), $n_1 = 8, n_2 = 10$, where the dipole variation has $\alpha = 0.7$, $B = 0$, with positive cosmological constant $\Lambda = 0.1$, and the initial density given by the constant function in (54). This model is axially symmetric since $P = Q = 0$. The black line is the geometric horizon, which appears initially at the $r = 1$ worldline at $t = t_0$, and all interior worldlines collapse to a geometric horizon after the initial data. No cosmological horizon is shown for the range of times given, but occurs earlier in the spacetime. All shell crossings appear after the formation of the horizon in this configuration. Similar to figure (1), we choose the directions along the maximum and the LTB subcase to show the 'earliest' shell crossing times. Shell crossings appear after the formation of the geometric horizons along each worldline.

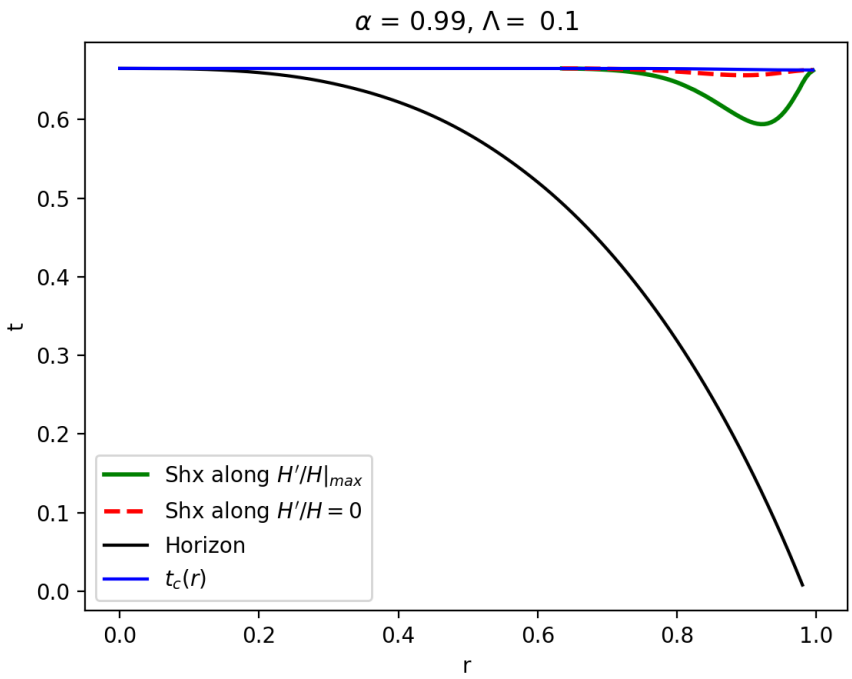

Figure 3: Model with $E(r)$ given by equation (51), $n_1 = 8, n_2 = 10$, where the dipole variation has $\alpha = 0.99$, $B = 0$, with positive cosmological constant $\Lambda = 0.1$, and the initial density given by the constant function in (54). This model is axially symmetric since $P = Q = 0$. The shell crossing profiles significantly deviate from the LTB models but the horizons still appear before the shell crossings along every worldline. This shows clearly that Szekeres model dipole functions are very important when it comes to shell crossings, as Szekeres models are more prone to shell crossings due to these dipole variations. The Szekeres and LTB shell crossings are censored by a geometric horizon, and as $\alpha \to 1$, the shell crossings and geometric horizons will overlap on the initial data surface.

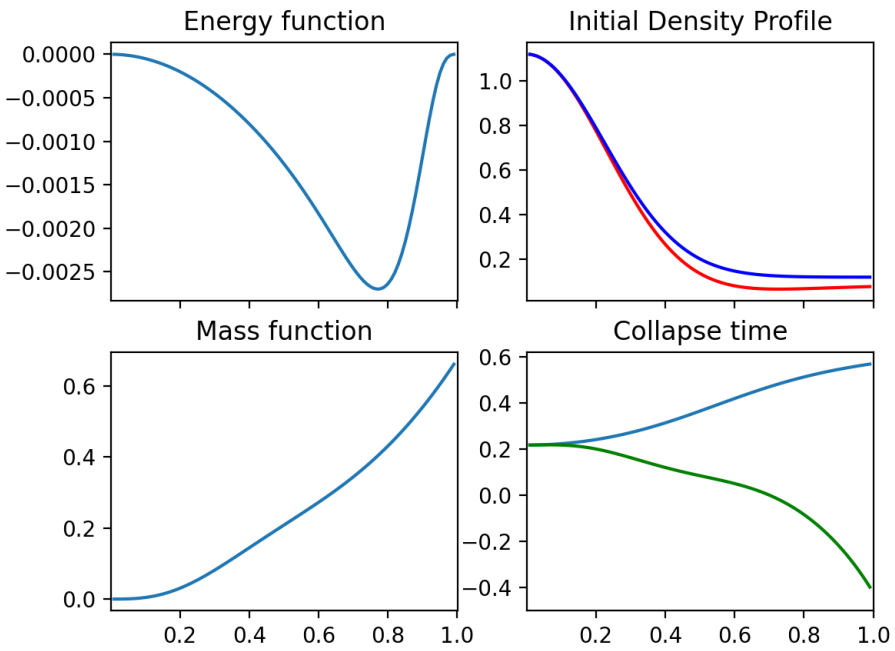

Figure 4: This model has $E(r)$ from equation (51), with a gaussian density profile from equations (54) with $a = 1, b = 10, c = 3/\kappa$, and $\Lambda = 0.1$. All horizontal axes are the radial coordinate for each worldline in the collapsing region. The LTB density profile is in blue, and the density profile along the maximal dipole direction is in red, where the dipole term has $\alpha = 0.5$. The cosmological horizon exists but is not plotted. The geometric horizon is plotted on the collapse time graph in green (bottom right panel), along with the collapse time of each worldline in blue. No shell crossings appear in this model since $t_c'(r) \geq 0$ in the domain of r.

Figure 1 shows a model where the shell crossings are not censored by any horizons. In Figures 2 and 3, the same model with different dipole terms is shown, to see the effect of the dipole on the appearance of the shell crossings. Both models share the same collapse times, horizon locations, and LTB shell crossing profiles, and only differ in the parameter α, which greatly affects the appearance time of the Szekeres maximal dipole shell crossing (the shell crossing along the direction of the maximum of H'/H). Figure 4 shows a variant of the model with a gaussian density profile, where the shell crossings do not appear anywhere in the domain, the cosmological horizon appears at an earlier time in the solution, and is not plotted. The focus on these pictures is the detection of the horizon and the comparison to the detection of the shell crossings along each worldline, and are strictly a qualitative example of the applications of the Cartan method, rather than physical models of collapse.

7 Discussion

We have presented the full invariant characterization of the quasi-spherical Szekeres models with positive cosmological constant. And we have described series of models of black hole formation in the Szekeres spacetime that may contain shell crossings. The shell crossings, when they do appear, as well as the geometric horizons, can be located by using the scalar curvature invariants derived by the Cartan-Karlhede algorithm. These horizons can sometimes appear before shell crossings in solutions, and when dealing with the case $E(r) < 0$, any model construction that has shell crossings needs to be inspected numerically (see Figures 1, 3, 2). The case where $E(r) = 0$ presents a way to exactly solve the Friedmann-like equations for the spacetime, and can be used for matching conditions where a region with $E(r) < 0$ is matched to a region where $E(r) \geq 0$. For example, we may wish to match the interior spacetime where the black hole is forming to an exterior Schwarzschild spacetime. Alternatively, in cosmology we may like to match the black hole forming region to an outer FLRW model. The Szekeres models allows us to describe complicated formation processes in an actual background cosmology, something that isn't possible in a more restrictive model without approximations. The models presented give a natural way to build up a spacetime to describe black holes, or galactic black holes [6], and match these models to a desired exterior.

It is expected that the occurrence of shell crossings in these dust models is simply an indicator of a breakdown of the model, and that an inclusion of a pressure term would either prevent their formation, or delay them during the collapse. In more general Szekeres-Szafron models with a perfect fluid source, there is the possibility of including a homogeneous pressure term, $p(t)$ to the model, which modifies the Friedmann and density equations. With these more general perfect fluid sources, choosing a valid equation of state is a more difficult problem, as the Szekeres models are not compatible with common equations of state used in applications such as a barotropic equation of state. It has been shown that in an invariant coframe as determined by the Cartan-Karlhede algorithm, certain features of the curvature tensors allow for the detection of invariantly defined surfaces, like the geometric horizons. These geometric horizons coincide with the traditional apparent horizons in the Szekeres spacetime, allowing for an invariant way to characterize any applications of these models to black hole formation, structure formation, or any other conceived physical application. This carries forward into the non-zero cosmological constant case, and future extension of the invariant classification of the Szekeres-Szafron spacetime with pressure included would be a logical step forward.

In general, to show that a shell crossing is properly censored behind a horizon, we need to check that any path starting inside the horizon cannot escape for all time. A common way to do this is to integrate the geodesic equations for light emitted inside the horizon, and show that all null geodesics stay inside the horizon. For these Szekeres models, this needs to be checked numerically, and work done by Hellaby et al [15], and Krasinski and Bolejko [17] has show that, in general, this is difficult, as it is a numerically intensive process even with $\Lambda = 0$. In comparison to this other work, the models constructed here admit shell crossings in a collapsing region of spacetime where the shell crossing region is always contained within a geometric horizon. The time of appearance of the geometric horizon along a particular worldline can always be forced to happen before the time of the appearance of the shell crossings, by choosing the set of arbitrary functions accordingly. The models considered here are on a restricted domain where the geometric horizons are always covering the entire region where shell crossings occur. This means that the shell crossings in these models, since they appear behind a geometric horizon, are censored, and thus the model behaviour

outside the horizon is not affected by the shell crossings inside the horizon.

Szekeres-Szafron models are generalizations of the Szekeres model where the solution is no longer a dust, but admits a time dependent (homogeneous) pressure term. These models would be more suited to accurately describe the properties of the formation of black holes through collapse with a perfect fluid, and are part of future investigation. The notion that a Szekeres model with zero pressure correctly describes the process of collapse is, of course, only an approximate one, and extending the problem to Szekeres-Szafron models might qualitatively change the way the formation process occurs. With respect to the shell crossings, the pressure between the worldlines might delay or prevent shell crossing occurrence altogether. An examination of the dynamics of collapse of a perfect fluid with a homogeneous pressure term in the Szekeres models is a topic of future work.

Acknowledgements

We would like to thank Ismael Delgado Gaspar for fruitful discussions on the topic throughout this project. This work was supported by NSERC (A.A.C).

Declarations

All datasets generated and analysed during this study are available from the corresponding author on request.

References

[1] J. D. Barrow and J. Stein-Schabes. Inhomogeneous cosmologies with cosmological constant. *Physics Letters A*, 103(6):315–317, July 1984.

[2] K. Bolejko, M. Célérier, and A. Krasiński. Inhomogeneous cosmological models: exact solutions and their applications. 28(16):164002, August 2011. Publisher: IOP Publishing.

[3] I. Booth. Black-hole boundaries. *Canadian Journal of Physics*, 83(11):1073–1099, 2005.

[4] S. Chakraborty and U. Debnath. Shell Crossing Singularities in Quasi-Spherical Szekeres Models. *Gravitation and Cosmology*, 14(2):184–189, April 2008.

[5] A Coley, R Milson, V Pravda, and A Pravdová. Classification of the weyl tensor in higher dimensions. *Classical and Quantum Gravity*, 21(7):L35–L41, March 2004.

[6] A. A. Coley, N. Layden, and D. D. McNutt. An invariant characterization of the quasi-spherical Szekeres dust models. *General Relativity and Gravitation*, 51(12):164, December 2019.

[7] A. A. Coley, D. D. McNutt, and A. A. Shoom. Geometric Horizons. *Physics Letters B*, 771:131–135, August 2017.

[8] U. Debnath, S. Nath, and S. Chakraborty. Quasi-spherical collapse with cosmological constant. *Mon. Not. Roy. Astron. Soc.*, 369:1961–1964, 2006.

[9] G. F. R. Ellis, R. Maartens, and M. A. H. MacCallum. *Relativistic Cosmology*. Cambridge University Press, Cambridge, 2012.

[10] I. D. Gaspar, J. C. Hidalgo, R. A. Sussman, and I. Quiros. Black hole formation from the gravitational collapse of a non-spherical network of structures. *Physical Review D*, 97(10):104029, May 2018.

[11] S. M. C. V. Goncalves. Strong curvature singularities in quasispherical asymptotically de Sitter dust collapse. *Classical and Quantum Gravity*, 18(21):4517–4530, November 2001.

[12] T. Harada and S. Jhingan. Spherical and nonspherical models of primordial black hole formation: exact solutions. *Progress of Theoretical and Experimental Physics*, 2016(9):093E04, September 2016.

[13] T. Harada, C. Yoo, T. Nakama, and Y. Koga. Cosmological long-wavelength solutions and primordial black hole formation. *Physical Review D*, 91(8):084057, April 2015.

[14] C. Hellaby. Modelling Inhomogeneity in the Universe. October 2009.

[15] C. Hellaby and A. Krasinski. You Can't Get Through Szekeres Wormholes - or - Regularity, Topology and Causality in Quasi-Spherical Szekeres Models. *Physical Review D*, 66(8):084011, October 2002.

[16] A. Krasiński. Expansion of bundles of light rays in the Lema\ˆitre – Tolman models. *arXiv:2103.09624 [gr-qc]*, March 2021. arXiv: 2103.09624.

[17] A. Krasiński and K. Bolejko. Apparent horizons in the quasi-spherical Szekeres models. *Physical Review D*, 85(12):124016, June 2012.

[18] A. Krasiński and K. Bolejko. Geometry of the quasi-hyperbolic Szekeres models. *Physical Review D*, 86(10):104036, November 2012.

[19] R. A. Sussman and K. Bolejko. A novel approach to the dynamics of Szekeres dust models. *Classical and Quantum Gravity*, 29(6):065018, March 2012.

[20] D. A. Szafron. Inhomogeneous cosmologies: New exact solutions and their evolution. *Journal of Mathematical Physics*, 18(8):1673–1677, August 1977. Publisher: American Institute of Physics.

[21] P. Szekeres. A class of inhomogeneous cosmological models. *Communications in Mathematical Physics*, 41(1):55–64, February 1975.

[22] D. Vrba and O. Svitek. Modelling Inhomogeneity in Szekeres Spacetime. *General Relativity and Gravitation*, 46(10):1808, October 2014.

[23] J. Wainwright. Characterization of the Szekeres inhomogeneous cosmologies as algebraically special spacetimes. *Journal of Mathematical Physics*, 18(4):672–675, April 1977. Publisher: American Institute of Physics.